P H Y S I C A L   R E V I E W   L E T T E R S

Apparent Fracture in Polymeric Fluids Under Step Shear

Okpeafoh S. Agimelen and Peter D. Olmsted[*]

Soft Matter Physics Group, School of Physics and Astronomy, University of Leeds, Leeds LS2 9JT, United Kingdom

Recent step strain experiments in well-entangled polymeric liquids demonstrated a bulk fracturelike phenomenon. We study this instability by using a modern version of the Doi-Edwards theory for entangled polymers, and we find close quantitative agreement with the experiments. The phenomenon occurs because the viscoelastic liquid is sheared into a rubbery state that possesses an elastic constitutive instability [G. Marrucci and N. Grizzuti, J. Rheol. **27,** 433 (1983)]. The fracture is a transient manifestation of this instability, which relies on the amplification of spatially inhomogeneous fluctuations. This mechanism differs from the fracture in glassy materials and dense suspensions.

PACS numbers: 47.50.Cd, 47.20.Gv, 47.50.Gj, 83.60.Wc

Introduction.—Viscoelastic liquids have slow time scales due to the relaxation of internal degrees of freedom such as polymer deformation or the structures of self-assembled materials such as amphiphiles. These slow time scales give rise to dramatic effects, such as rubbery behavior at high deformation rates, viscous behavior at lower rates, and *both* solidlike and liquidlike features. Materials such as amorphous solid polymers [1] or metallic glasses [2] have arguably the most dramatic behavior possible for a solid: rupture, fracture, and flow at a macroscopically sharp interface. This has been modeled as collective rupture of shear transformation zones [3] and in dense colloidal materials as due to the coupling between shear and density [4].

Recent experiments have demonstrated fracturelike behavior in well-entangled polymeric *liquids*. Very rapid step strains were applied to polymer melts [e.g., poly(styrene-butadiene) [5] or poly(ethylene oxide) [6]] with $Z \approx 53$–160 entanglements per polymer. At such high shear rates, the liquid becomes rubbery and solidlike. After the step strain the solidlike melt relaxes homogeneously for a short time, followed by a rapid relaxation during which the material splits into two layers moving in opposite directions, separated by a thin ($\lesssim 40\ \mu$m) shear band or "fracture" layer [Fig. 1 of Ref. [5]]. Reference [5] suggested that this is due to microscopic yield, such as a sudden localized chain pullout or loss of entanglements, perhaps analogous to the shear transformation zone picture for yield in amorphous solids [4].

We show that these results can be explained by a pure constitutive instability due to the effects of shear flow on the elastic stress in the fluid, and it is actually contained in the Doi-Edwards (DE) theory of entangled polymers [7–9]; this provides yet another mechanism for fracture, due purely to a constitutive shear instability in a viscoelastic liquid brought suddenly into a (transient) solid state.

The motion of an entangled polymer is restricted to a tubelike region due to the constraints imposed by surrounding chains. The DE theory for this [7] predicts a maximum in the shear stress T_{xy} as a function of shear rate [Fig. 1(a)],

at a shear rate $\dot{\gamma}$ roughly equal to the reciprocal of the time τ_d for a polymer to diffuse (or reptate) along its tube. This nonmonotonic constitutive behavior (which was not inferred in early experiments on polymer melts [10]) indicates instability, which can lead to inhomogeneous flows and *shear banding* [11]. This constitutive instability was widely implicated [12] in the spurt effect [13], responsible for instabilities in industrial processes; however, spurt is now usually attributed to wall slip [14]. In rapid startup flow, the DE theory predicts the rubbery behavior of a stress overshoot [7–9]. Modern theories incorporate chain stretch and convected constraint release—chain relaxation due to the release of entanglement constraints, which restores stable constitutive behavior [15]. However, new observations of shear banding seem to validate the DE instability [9,16,17] in some cases. We will show that apparent fracture is another manifestation of the DE instability.

Model.—We separate the total stress tensor **T** into contributions from the polymer and a Newtonian solvent, as $\mathbf{T} = G\mathbf{W} + \eta(\boldsymbol{\kappa} + \boldsymbol{\kappa}^T) - p\mathbf{I}$, where G is a modulus, η is the solvent viscosity, the pressure p maintains incompressibility, **I** is the identity tensor, and $\kappa_{\alpha\beta} = \boldsymbol{\nabla}_{\beta} v_{\alpha}$. The fluid velocity **v** (with no slip boundary conditions) with mass density ρ obeys

$$\rho \frac{d\mathbf{v}}{dt} \equiv \rho \left[\frac{\partial}{\partial t} + (\mathbf{v} \cdot \nabla) \right] \mathbf{v} = \nabla \cdot \mathbf{T}, \qquad (1)$$

where $\nabla \cdot \mathbf{T} = 0$ for very small Reynolds numbers, as is the case here. The dimensionless polymeric conformation, or strain, tensor **W** is assumed to obey the diffusive Rolie-Poly model [9,18]:

$$\frac{d\mathbf{W}}{dt} = \boldsymbol{\kappa} \cdot \mathbf{W} + \mathbf{W} \cdot \boldsymbol{\kappa}^T - \frac{1}{\tau_d}(\mathbf{W} - \mathbf{I}) - \frac{2\left(1 - \sqrt{\frac{3}{\mathrm{Tr}\mathbf{W}}}\right)}{\tau_R}$$
$$\times \left(\mathbf{W} + \beta\sqrt{\frac{3}{\mathrm{Tr}\mathbf{W}}}(\mathbf{W} - \mathbf{I}) \right) + \mathcal{D}\nabla^2\mathbf{W}, \qquad (2)$$
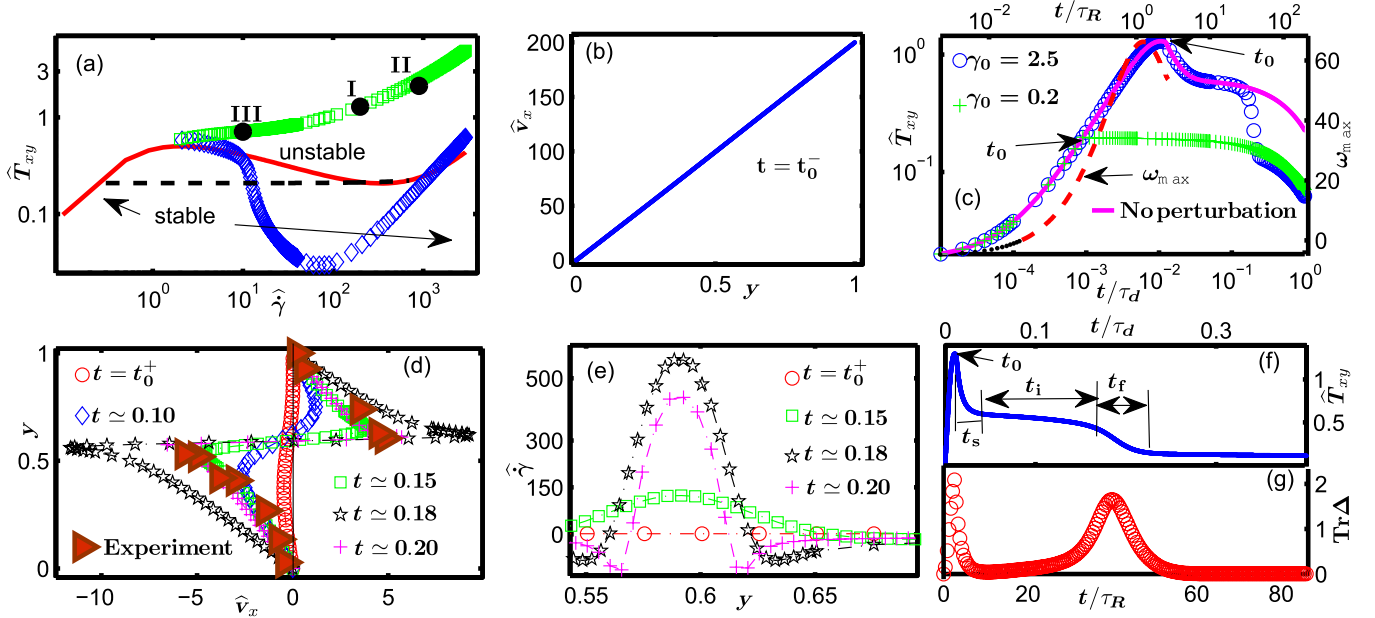
FIG. 1 (color online).   (a) Constitutive (solid line) and steady state shear banding (black dashes) curves. The stress overshoot is indicated by green squares; small perturbations grow exponentially in time ($\omega_{max} > 0$) for stresses exceeding the stress given by the blue diamonds. The stresses at t_0 for three cases described in the text are indicated by I, II, and III. (b) Velocity profile at t_0^- (just before shear cessation) for $\langle \hat{\gamma} \rangle = 200$. (c) Stress relaxation for step strains $\gamma_0 = 0.2, 2.5$; the solid line is for $\gamma_0 = 2.5$ with no initial perturbation. The dot-dashed line shows the evolution of the most unstable eigenvalue ω_{max}, which becomes unstable ($\omega_{max} > 0$) in the red (dashed) region. (d) Velocity profiles during fracture, with experimental data from [5] superposed. (e) Shear rate profiles, (f) stress relaxation, and (g) evolution of the maximum stretch in the gap Tr$\mathbf{\Delta}^{max}$. [Parameters: $Z = 72$, $\tau_R = \tau_d/216$, $\langle \hat{\gamma} \rangle = 200$, $\gamma_0 = 2.5$, $t_0 = 0.01250\tau_d$, and $t_0^{\pm} = t_0 \pm 10^{-5}\tau_d$. Times t and $1/\omega_{max}$ are displayed in units of τ_d.]

which is a simplified form of the Graham-Likhtman-Milner-McLeish (GLaMM) model, itself a modern version of Doi-Edwards theory [19]. Here, τ_d is the reptation time, and the Rouse time τ_R governs the relaxation of stretch Tr($\mathbf{W}$). The parameter β quantifies convected constraint release; a large value of β corresponds to more convected constraint release, which leads to monotonic (stable) behavior of the shear stress. Spatial gradients due to stress "diffusivity" $\mathcal{D}$ are subject to the boundary condition $\nabla \mathbf{W} = 0$ [11].

Calculations.—We consider two infinite flat plates separated by $L\hat{\mathbf{y}}$ where the top plate moves parallel to $\hat{\mathbf{x}}$ and the bottom plate is fixed. The velocity field is thus given by $\mathbf{v} = v_x(t, y)\hat{\mathbf{x}}$, and $\mathbf{W} \equiv \mathbf{W}(t, y)$. We define dimensionless quantities $\hat{\gamma} = \dot{\gamma}\tau_d$, $\hat{\mathcal{D}} = \mathcal{D}\tau_d/L^2$, $\epsilon = \eta/(G\tau_d)$, $\hat{\rho} = \rho L^2/(G\tau_d^2)$, $\hat{v} = \tau_d v/L$, and $\hat{t} = t/\tau_d$. The degree of entanglement Z determines the Rouse time via $\tau_R = \tau_d/(3Z)$ [18,19]. A desired average shear rate is imposed for a duration t_0 leading to a strain $\gamma_0 = \langle \hat{\gamma} \rangle t_0$.

The values $\tau_d = 310$ s and $Z = 55$–100 are consistent with the data in [5]; with $\eta \approx 1$ Pa s and $G \approx 7 \times 10^3$ Pa [20] we find $\epsilon \approx 10^{-7}$; for numerical stability, we use $\epsilon = 10^{-4}$. For $L = 1$ mm, $\rho \approx 10^3$ kg m^{-3} gives $\hat{\rho} \approx 10^{-10}$, and we use $\hat{\mathcal{D}} = 10^{-5}$ [21]. Spatial derivatives are discretized by using a semi-implicit central finite difference scheme. For a time step $\delta\hat{t} = 10^{-6}$ and 1000 spatial mesh points, the maximum velocity in the fracture and time to fracture converge within a few percent.

We infer (in)stability by considering the evolution of perturbations to the uniform solution to Eq. (2): $\mathbf{s}(t) \equiv [\Delta_{xx}, \Delta_{xy}, \Delta_{yy}](t)$, where $\mathbf{\Delta} = \mathbf{W} - \mathbf{I}$, with initial conditions $\mathbf{s}(0) = [0, 0, 0]$ and imposed uniform shear rate $\hat{\gamma}$. At some time t_0 we impose an inhomogeneous perturbation $\delta\mathbf{u}(y, t_0) = [\delta\hat{\gamma}, \delta\Delta_{xx}, \delta\Delta_{xy}, \delta\Delta_{yy}](y, t_0) = \sum_k \delta\mathbf{u}_k(t_0) \exp(iky)$. The full dynamics is thus given by $\mathbf{u}(y, t; t_0) = [\hat{\gamma}, \mathbf{s}](t_0) + \delta\mathbf{u}(y, t - t_0)$. The perturbation $\delta\mathbf{u}$ evolves for small times $t - t_0$ according to the dynamics given by linearizing Eqs. (1) and (2): $\delta\dot{\mathbf{u}}_k(t - t_0) = \mathsf{M}_k[\mathbf{s}(t_0)]\delta\mathbf{u}_k(t - t_0)$. The growth or decay of this perturbation at early times indicates whether the perturbation can induce fracture after shearing is stopped at t_0. The perturbation will grow after t_0 when the largest real part ω_{max} of the spectrum of eigenvalues of M_k is positive.

To capture the behavior reported in [5], we consider a fluid with nonmonotonic constitutive behavior, $\beta = 0$ [solid line in Fig. 1(a)], and use $Z = 72$ (consistent with [5]); this leads to shear banding and a stress plateau in the steady state [dashes in Fig. 1(a)] [11]. We initialize Eq. (2) with random perturbations $\delta\mathbf{u}(0, y) = \xi\sum_{n=1}^{5}(\mathbf{A}_n/n^2) \times \cos n\pi y$, $A_{ni} \in [-1, 1]$, where i are the four components of $\mathbf{A}_n$; here, ξ sets the scale of the perturbation. The penalty $1/n^2$ arises because high wave numbers n should be suppressed by both spatial gradients in $\mathbf{W}$ and by the slow dynamics of long wavelength velocity fluctuations that induce perturbations upon sample loading (for

example). We use $\xi = 0.01$, consistent with the scale of typical thermal fluctuations in **W** [22].

Perturbations can grow if the fluid becomes unstable [8,22–24]. For 34% of 300 sets of randomly chosen $\mathbf{A}_n$, the resulting velocity profiles were similar to those reported in [5]. Using initial conditions that produce the experimentally observed velocity profile, we simulate examples reported in [5]. The green squares in Fig. 1(a) are the overshoot stresses at different shear rates, and the stresses at t_0 for the three cases studied are indicated as I, II, and III. For times t_0 later than the time at which the startup stress is given by the blue diamonds, the perturbation $\delta \mathbf{u}$ grows exponentially upon shear cessation. This is where we infer instability.

Case I.—For $\langle\dot\gamma\rangle\tau_R \approx 1$ and $\gamma_0 > \gamma_{ov}$ (the overshoot strain), we impose $\langle\hat\gamma\rangle = 200$ ($\langle\dot\gamma\rangle\tau_R = 0.93$) for $\gamma_0 = 2.5$. Immediately before cessation at t_0^-, the velocity profile is imperceptibly inhomogeneous [Fig. 1(b)], while at t_0^+ the fluid has stopped with a slight inhomogeneity induced by the perturbation [Fig. 1(d)]. Some stress then quickly relaxes due to stretch relaxation in a time $t_s \simeq 7\tau_R$ [Figs. 1(c), 1(f), and 1(g)], followed by an induction time $t_i \simeq 30\tau_R$ with relaxation due to reptation [blue circles in Figs. 1(c) and 1(f)]. The perturbation slowly grows during t_i and localizes, leading to a fracture plane at which the fluid shears very rapidly [Figs. 1(d) and 1(e)], and a sizable stretch Tr$\boldsymbol{\Delta}$ is induced [Fig. 1(g)]. The stress relaxes quickly during this localization in a time $t_f \simeq 15\tau_R$ [Figs. 1(c) and 1(f)]. Thereafter it relaxes like a quiescent melt with a small initial strain $\gamma_0 = 0.2$ [Fig. 1(c)]. Since the boundaries are fixed, positive shear strain within the slip layer is balanced by opposing recoil in the still-entangled outer regions [e.g., Fig. 1(e) for $t/\tau_d > 0.15$]. Without an initial perturbation, only quiescent relaxation is obtained [solid line in Fig. 1(c)]. The velocity profiles [Fig. 1(d)] are consistent with Fig. 1 of Ref. [5] (which has an induction time $t_i \approx 5\tau_R$).

Stability.—Figures 1(a) and 1(c) suggest that the material is unstable ($\omega_{max} > 0$) from well before the stress overshoot until shear cessation. To understand this instability, we turn to the Marrucci-Grizzuti observation that for strain $\gamma_0 \gtrsim 2.1$ the elastic energy function $F(\gamma)$ for the DE model has a negative effective shear modulus $\mathcal{A} \equiv \partial^2 F/\partial\gamma^2 < 0$ [8], which heralds instability. Marrucci and Grizzuti predicted elastic instability for a step strain, for

$$\mathcal{A}^{\text{eff}} \equiv \mu(t_0 + t_s)\frac{\partial^2 F}{\partial\gamma^2}\bigg|_{\gamma_0} + [1 - \mu(t_0 + t_s)]\frac{\partial^2 F}{\partial\gamma^2}\bigg|_0 < 0, \quad (3)$$

where $\mu(t)$ is the fraction of unrelaxed material. The elastic limit $\dot\gamma\tau_d \gg 1$ gives $\mathcal{A}^{\text{eff}} \simeq \partial T_{xy}/\partial\gamma = \dot\gamma^{-1}\partial T_{xy}/\partial t < 0$ [8,17,22,23], which coincides with the stress overshoot.

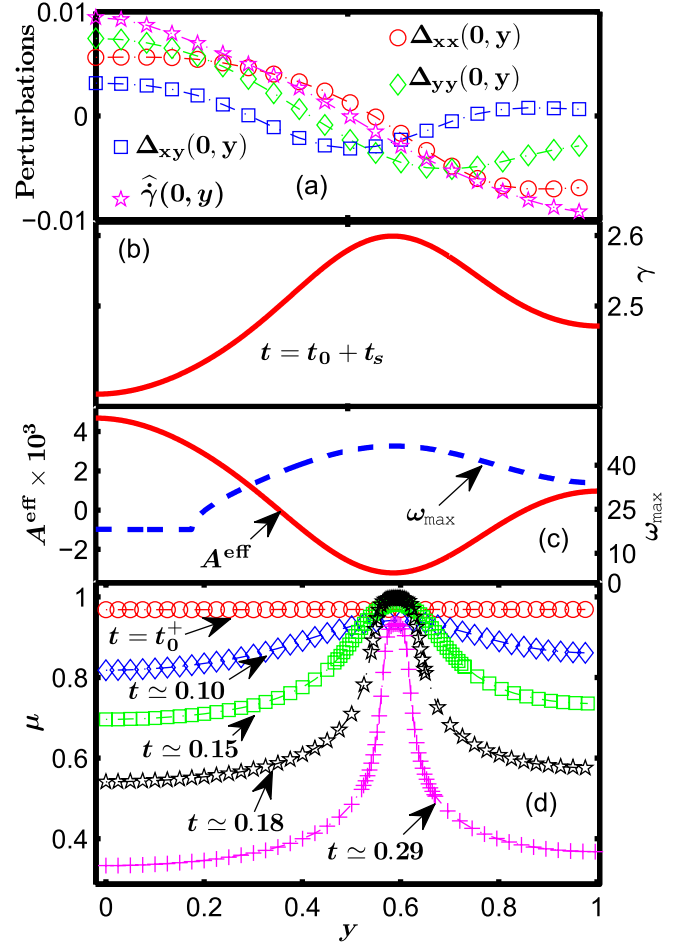FIG. 2 (color online). Spatial profiles of (a) initial perturbation, (b) local strain, and (c) effective modulus $\mathcal{A}^{\text{eff}}$ as well as the unstable growth rate ω_{max}, after cessation of flow and subsequent stretch relaxation. (d) Evolution of unrelaxed polymer segments $\mu(y, t)$ during fracture development. [Parameters are as in Fig. 1. Time t is displayed in units of τ_d.]

The anisotropy of the polymer conformation tensor **W** defines $\mu \equiv |\lambda_1 - \lambda_2|/|\lambda_1 + \lambda_2|$, where λ_i are the eigenvalues of **W** in the plane containing the velocity gradient and flow directions [25]. For a homogeneous initial condition, $\mu(t)$ relaxes homogeneously to zero, while an inhomogeneous initial condition initiates instability and an inhomogeneous $\mu(y, t)$ [Fig. 2(d)].

Figures 2(d) and 2(c) show the spatial profiles for the strain and the effective shear modulus $\mathcal{A}^{\text{eff}}$ after stretch relaxation [26]. The fracture region is most unstable, so that the initial perturbation [Fig. 2(a)] can localize strain. The unstable region predicted by the elastic limit coincides with the most unstable eigenvalue ω_{max} calculated from the full dynamics, which indicates instability before the stress overshoot is reached [e.g., Fig. 1(a)] because of the viscous contribution to the instability [23]. The most unstable eigenvector is dominated by the growth of Δ_{xx} [24], which enhances stretch in the flow direction.
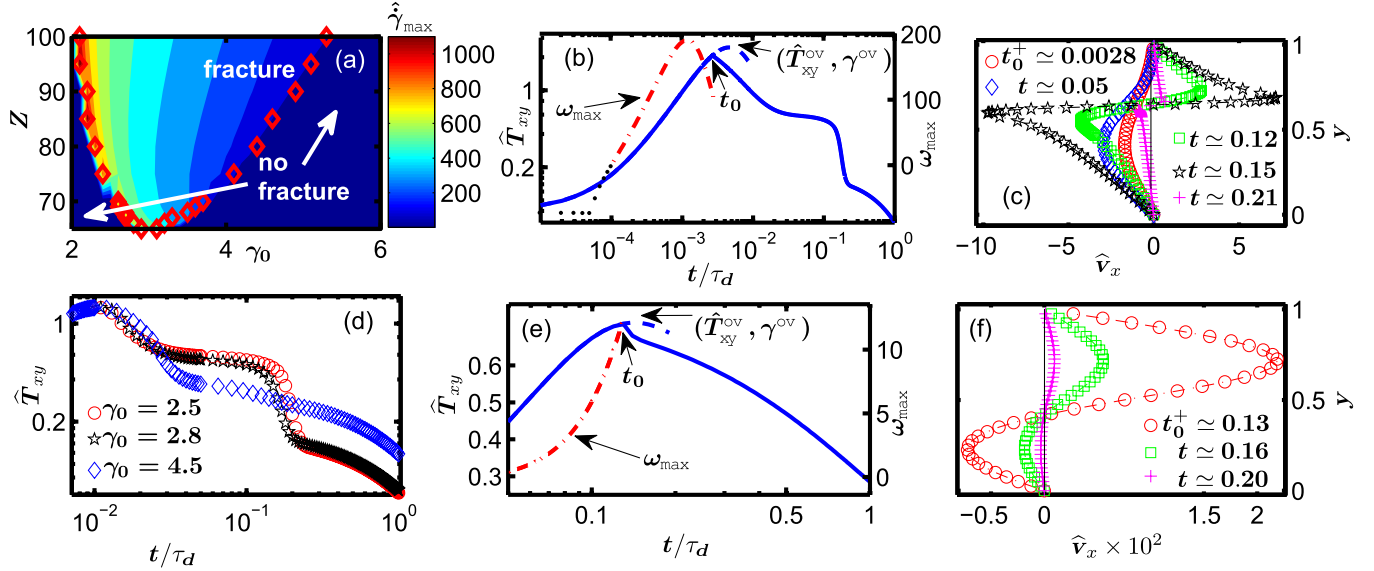
FIG. 3 (color online). (a) Values of Z and γ_0 required for fracture at fixed $\langle \hat{\gamma} \rangle$; contours show the maximum local shear rates during fracture. (b), (c) Case II ($\langle \hat{\gamma} \rangle = 900$, $\langle \dot{\gamma} \rangle \tau_R = 4.2$, $\gamma_0 = 2.5$): (b) stress relaxation and unstable growth rate ω_{max} (the dashed line is the stress overshoot with no initial perturbation); (c) velocity profiles during fracture. (d) Stress decay for three different imposed strains γ_0. (e), (f) Case III ($\langle \hat{\gamma} \rangle = 10$, $\langle \dot{\gamma} \rangle \tau_R = 0.046$, $\gamma_0 = 1.3$): (e) stress relaxation and ω_{max} and (f) velocity profiles. [All other parameters are as in Fig. 1. Time t is displayed in units of τ_d.]

Conditions for fracture.—A detailed study shows that perturbations in Δ_{xx} and Δ_{yy} induce fracture [24]. The step strain γ_0 advects the initial perturbation into a shear component of the polymer strain (e.g., $W_{xy}(y, t_0) \simeq \gamma_0[1 + \Delta_{yy}(y, 0)]$), which generates an inhomogeneous shear rate $\delta \hat{\dot{\gamma}}(y, t_0^+) \simeq -\gamma_0 \Delta_{yy}(y, 0)/\epsilon$ immediately after cessation of flow to maintain $\nabla \cdot \mathbf{T} \simeq 0$. Although general perturbations are complex [Fig. 2(a)] [24], a local maximum in the *polymeric strain* γ defines the position with the most negative effective shear modulus $\mathcal{A}_{eff} < 0$ and the fastest growth rate ω_{max} [Fig. 2(c)] [26] and, thus, the fracture position.

The subsequent evolution resembles spinodal decomposition of a conserved quantity, since the total strain γ_0 is fixed. The strain in the most unstable region grows, while that in the less unstable regions decreases. This leads to recoil and a sharpening of the deformation around the most unstable position, which can then fracture if the initial amplitude grows quickly enough compared to the overall relaxation due to reptation. Significant convected constraint release suppresses fracture because of the enhanced relaxation.

Character of fracture.—A larger strain leads to a less dramatic fracture [Figs. 3(a) and 3(d)], because the total stress has passed the overshoot and decreased, hence releasing less stress into the fracture; however, the larger molecular strain W_{xy} leads to a faster growing instability, which is consistent with Fig. 8 of Ref. [5]. Alternatively, for a higher imposed strain rate and t_0 beyond the overshoot, the stretch-dominated response leaves less orientational stress and molecular strain after stretch relaxation, so that fracture takes longer to develop [23].

In case II ($\langle \hat{\gamma} \rangle = 900$, $\langle \dot{\gamma} \rangle \tau_R = 4.2$), the shear rate is large but the strain $\gamma_0 = 2.5$ is slightly less than the overshoot strain γ_{ov} [Figs. 3(b) and 3(c)]. The velocity profiles are consistent with Fig. 2 of Ref. [5]. Because the growth rate ω_{max} is so rapid for the high shear rate, the smaller strain can effect the necessary large growth of the instability. In this case, the induction time and velocity profiles are similar to case I. In case III ($\langle \hat{\gamma} \rangle = 10$, $\langle \dot{\gamma} \rangle \tau_R = 0.046$) the shear rate is relatively small [Figs. 3(e) and 3(f)], and fracture and recoil are very weak due to the small growth rate. The stress response due to the inhomogeneity is almost negligible compared to that of an unperturbed initial condition. The weak recoil agrees with Fig. 7 of Ref. [5].

Figure 6 of Ref. [5] demonstrated that, for subovershoot strains, higher shear rates lead to longer induction times, while our calculations predict shorter induction times because of the faster growing instability [24]. We cannot explain this discrepancy.

Conclusion.—We have shown that the fracture seen in recent step strain experiments on polymeric liquids [5,6] could result from an underlying elastic instability in the DE model, whose signature is stress overshoot during rapid startup [8,9,27]. Once stretch degrees of freedom have relaxed, the deformed melt is elastically unstable so that small inhomogeneities grow into plastic strain (shear flow) in the most unstable regions. If this instability grows fast enough compared to reptation, then a dramatic fracture can result. The perturbation's shape and amplitude control whether fracture occurs.

In related works, Manning *et al.* studied a shear-transformation-zone model of an amorphous solid [3], demonstrating plastic yield within a fluid shear band (or

fracture) during startup of shear flow, while a shear-dilation coupling has been shown to lead to fracture in glass-forming materials [4]. In the rubbery polymer liquid considered here, the instability is purely constitutive: Shearing leads to a decreased stress as chains are oriented along the flow direction, and the resulting fluid is mechanically unstable.

Boukany, Wang, and Wang suggested that the fracture demands new physics [5]. Certainly, current tube models are incomplete [28]. However, our calculations are reasonable if spatial features are smooth on length scales greater than the tube diameter $a \simeq 3\text{–}4$ nm. For a gap of 1 mm, the fracture width $\delta x \simeq 0.05$ corresponds to a thickness of the order of 50 μm, which is consistent with the dimension ≤ 40 μm reported in Ref. [5]. Thus, higher experimental resolution will determine whether or not the continuum nature of the tube model is adequate.

---

*Corresponding author.
p.d.olmsted@leeds.ac.uk

[1] M. J. Doyle, A. Maranci, E. Orowan, and S. T. Stork, Proc. R. Soc. A **329**, 137 (1972).

[2] J. Lu, G. Ravichandran, and W. Johnson, Acta Mater. **51**, 3429 (2003).

[3] M. L. Manning, J. S. Langer, and J. M. Carlson, Phys. Rev. E **76**, 056106 (2007); M. L. Manning, E. G. Daub, J. S. Langer, and J. M. Carlson, Phys. Rev. E **79**, 016110 (2009).

[4] A. Furukawa and H. Tanaka, Nat. Mater. **8**, 601 (2009).

[5] P. E. Boukany, S.-Q. Wang, and X. Wang, Macromolecules **42**, 6261 (2009).

[6] Y. Fang, G. Wang, N. Tian, X. Wang, X. Zhu, P. Lin, G. Ma, and L. Li, J. Rheol. **55**, 939 (2011).

[7] M. Doi and S. F. Edwards, *The Theory of Polymer Dynamics* (Oxford University, Oxford, 1989).

[8] G. Marrucci and N. Grizzuti, J. Rheol. **27**, 433 (1983); F. A. Morrison and R. G. Larson, J. Polym. Sci. B **30**, 943 (1992).

[9] J. M. Adams and P. D. Olmsted, Phys. Rev. Lett. **102**, 067801 (2009); J. Cao and A. E. Likhtman, *ibid.* **108**, 028302 (2012).

[10] E. V. Menezes and W. W. Graessley, J. Polym. Sci., Polym. Phys. Ed. **20**, 1817 (1982).

[11] N. A. Spenley, M. E. Cates, and T. C. B. McLeish, Phys. Rev. Lett. **71**, 939 (1993); P. D. Olmsted, Rheol. Acta **47**, 283 (2008); C.-Y. D. Lu, P. D. Olmsted, and R. C. Ball, Phys. Rev. Lett. **84**, 642 (2000).

[12] T. W. Huseby, J. Rheol. **10**, 181 (1966); Y. H. Lin, J. Rheol. **29**, 605 (1985); T. C. B. McLeish and R. C. Ball, J. Polym. Sci. B **24**, 1735 (1986); T. C. B. McLeish, *ibid.* **25**, 2253 (1987); D. S. Malkus, J. A. Nohel, and B. J. Plohr, SIAM J. Appl. Math. **51**, 899 (1991); M. M. Denn, Annu. Rev. Fluid Mech. **22**, 13 (1990).

[13] G. V. Vinogradov, A. Ya. Malkin, Yu. G. Yanovskii, E. K. Borisenkova, B. V. Yarlykov, and G. V. Berezhnaya, J. Polym. Sci., A-2, Polym. Phys. **10**, 1061 (1972).

[14] F. J. Lim and W. R. Schowalter, J. Rheol. **33**, 1359 (1989); S. Q. Wang, in *Polymers in Confined Environments*, Adv. Polym. Sci. Vol. 138 (Springer, Berlin, 1999), pp. 227–275; M. M. Denn, Annu. Rev. Fluid Mech. **33**, 265 (2001).

[15] G. Ianniruberto and G. Marrucci, J. Non-Newtonian Fluid Mech. **65**, 241 (1996); D. W. Mead and R. G. Larson, Macromolecules **31**, 7895 (1998).

[16] Y. T. Hu, L. Wilen, A. Philips, and A. Lips, J. Rheol. **51**, 275 (2007); S. Ravindranath, S.-Q. Wang, M. Olechnowicz, and R. Quirk, Macromolecules **41**, 2663 (2008); P. Tapadia, S. Ravindranath, and S.-Q. Wang, Phys. Rev. Lett. **96**, 196001 (2006); Y. T. Hu, J. Rheol. **54**, 1307 (2010).

[17] J. M. Adams and P. D. Olmsted, Phys. Rev. Lett. **103**, 219802 (2009); S.-Q. Wang, *ibid.* **103**, 219801 (2009).

[18] A. E. Likhtman and R. S. Graham, J. Non-Newtonian Fluid Mech. **114**, 1 (2003).

[19] R. S. Graham, A. E. Likhtman, T. C. B. McLeish, and S. T. Milner, J. Rheol. **47**, 1171 (2003).

[20] P. Tapadia and S.-Q. Wang, Phys. Rev. Lett. **91**, 198301 (2003).

[21] J. M. Adams, S. M. Fielding, and P. D. Olmsted, J. Non-Newtonian Fluid Mech. **151**, 101 (2008).

[22] J. M. Adams, S. M. Fielding, and P. D. Olmsted, J. Rheol. **55**, 1007 (2011).

[23] R. L. Moorcroft and S. M. Fielding, Phys. Rev. Lett. **110**, 086001 (2013).

[24] See Supplemental Material at http://link.aps.org/supplemental/10.1103/PhysRevLett.110.204503 for details about the stability calculation, the effects of different initial conditions, and movies.

[25] The definition of unrelaxed segments $\mu(t)$ matches the linear relaxation function $G(t) \equiv \lim_{\gamma_0 \to 0} T_{x,y}(t, \gamma)/\gamma_0$, as does the equivalent function used by Marrucci and Grizzuti for the DE model [8].

[26] Following Ref. [8], we use the stored free energy due to the orientational distribution of tube segments, given within the independent alignment approximation by $F(\gamma) = 1/2 \int_0^1 \ln\{1/2(1 + \gamma^2 x^2 + [(x^2\gamma^2 - 1)^2 + 4\gamma^2 x^4]^{1/2})\}dx$.

[27] R. L. Moorcroft, M. E. Cates, and S. M. Fielding, Phys. Rev. Lett. **106**, 055502 (2011).

[28] A. E. Likhtman, J. Non-Newtonian Fluid Mech. **157**, 158 (2009).